Research Paper
Carbon Reports
Vol. 1 No. 4 2022 223-230

The role of alkali metal exchange in zeolite-templated carbon synthesis

Erin E. Taylor[a)], Dalton Compton[a)], Gary F. Wyss[b)] and Nicholas P. Stadie[a),*]

a) Department of Chemistry & Biochemistry, Montana State University: Bozeman, MT 59717, United States
b) Center for Advanced Materials Processing, Montana Tech: Butte, MT 59701, United States

Despite great efforts to achieve ideal atomistic packing of carbon in the pore networks of even the largest pore zeolites, templating inaccuracies are ubiquitous in all presently synthesized zeolite-templated carbon (ZTC) materials. Idealized models suggest that the long-sought schwarzite-like structures could in principle be obtained by zeolite templating if the appropriate zeolite template were chosen (*e.g.*, faujasite for D surface schwarzites) and if perfect template fidelity (insertion of a pristine layer of pure carbon directly on the surface of the zeolite) could be achieved. A requirement to achieve such structures is increased carbon density within the zeolite. We report the investigation of a series of alkali metal cation-exchanged zeolites to determine how the periodic trends in the group 1 elements influence zeolite templating, with a specific focus on the metric of structural packing density (SPD) as resolved by ex situ thermogravimetry. In a survey based on controlled synthesis temperature, time, and flow conditions, an increasing SPD was observed with decreasing cation size, an effect that is consistent with the increasing strength of cation-π interactions. This effect could be promising for future work to increase the SPD of ZTCs for the synthesis of closed-tube, schwarzite-like carbonaceous solids.

KEYWORDS : Zeolite-templated carbon, Cation-exchanged, Structural packing density, Microporous, Framework materials

1. Introduction

Graphite and diamond were the only known pure crystalline forms of carbon until the discovery of fullerenes in 1985 [1] ushered in the still active "era of carbon allotropes" [2]. Since then, carbon nanotubes [3] and graphene [4] were also discovered, leaving one missing constituent in the sp^2-hybridized series of carbon allotropes. Whereas fullerenes, carbon nanotubes, and graphene are 0-, 1-, and 2-dimensional network solids, respectively, a 3-dimensional network solid of sp^2-hybridized carbon has yet to be synthesized. One possibility is a class of theoretical materials referred to as schwarzites [5–9]: any of an infinite set of structures that carry the topology of one of the triply periodic minimal surfaces first described by Hermann Schwarz [10] and later augmented by Alan Schoen [11] (see **Fig. 1**).

One possible route to the synthesis of schwarzite-like materials is to insert carbon into a pre-existing ordered template that carries a minimal surface topology. Zeolites are a class of well-known crystalline aluminosilicate minerals with a diversity of microporous structures (each given a bold typeface 3-digit code such as **FAU** for faujasite) [12]; several zeolite framework types carry a triply periodic minimal surface topology (*e.g.*, **FAU** carries the D surface, **LTA** carries the P surface, *etc*.) [13]. Kyotani and coworkers pioneered the search for ordered carbonaceous solids templated within the microporous channels of a zeolite [14], resulting in the first successful zeolite-templated carbon (ZTC) [15] reported in 1997. **FAU** is one of the most effective zeolite templates for synthesizing ZTCs since its pore entrances are ~7.4 Å wide [12], allowing for facile impregnation with one or more carbon precursors, and is commercially available in a wide variety of Si:Al ratios. The ideal **FAU** structure carries the D surface topology and is made up of sodalite cages connected by hexagonal prisms of SiO_4 tetrahedra. Zeolites can undergo a substitution of tetravalent silicon with trivalent aluminum, requiring the introduction of an extra-framework charge balancing cation [16]. For example, **FAU** zeolites can be exchanged with a wide range of cations: most commonly Na^+, K^+, Ca^{2+}, NH_4^+, or H^+. The identity of the cation exchanged within the framework significantly influences the catalytic and functional properties of the zeolite [17]. An important recent breakthrough in the synthesis of ZTC was made by cation exchange with La^{3+} [18]. However, despite numerous reports otherwise [19–22], no experimental ZTC exists that has a carbon density that is high enough to be considered as a "closed-tube" (schwarzite-like) framework material [23]. An accurate atomistic description of experimental ZTC is shown in **Fig. 2**; significant advances would be needed in order to achieve a schwarzite-like solid via zeolite templating.

* Corresponding Author, E-mail: nstadie@montana.edu

(Received July 30, 2022, Accepted September 12, 2022)
(J-STAGE Advance published September 21, 2022)

https://doi.org/10.7209/carbon.010404

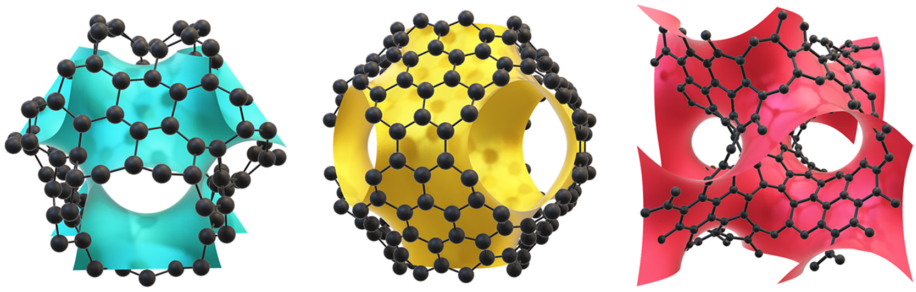

Fig. 1 From left to right: D766 schwarzite (black) overlaid on Schwarz D surface (blue), P8bal schwarzite (black) overlaid on Schwarz P surface (yellow), and G8bal schwarzite (black) overlaid on Schoen G surface (red).

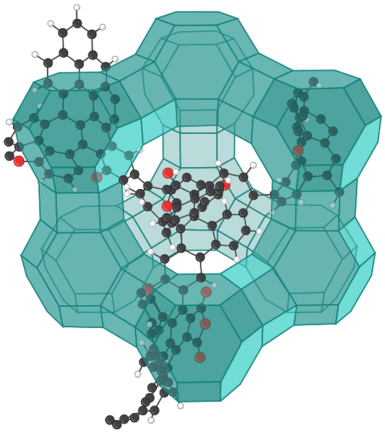

Fig. 2 Representative depiction of a blade-like subunit of ZTC confined within a supercage of an **FAU** zeolite. Carbon, oxygen, and hydrogen atoms are shown in black, red, and white, respectively. The T-sites (Si or Al) are shown as the vertices of a polyhedral depiction of **FAU** (teal lines and transparent faces) and zeolitic oxygen sites and cations are omitted for clarity.

The key requirement for realizing a schwarzite-like material via zeolite templating is to deposit carbon directly and exclusively on the inner walls of the zeolite pores, as opposed to randomly within the entire pore volume. To achieve this goal, the catalytic activity of the pore walls needs to be precisely tuned for the carbon precursor of choice. A metric that is useful in determining the templating fidelity of ZTCs is structural packing density (SPD), which can be calculated using thermogravimetric analysis (TGA). Together with powder X-ray diffraction (XRD) measurements to ensure that no carbon stacking occurred on the outer surfaces of the zeolite particles, TGA can indicate how much carbon (and other mass) was incorporated within the zeolite pore network. A specific SPD metric used herein is SPD_{cell}, which has been defined elsewhere as the mass of carbonaceous material within the zeolite divided by the mass of zeolite if it were an ideal pure silica variant [23]. Schwarzite-like ZTCs would necessarily exhibit a high SPD_{cell} of 0.63–0.71 $g_{ZTC}\, g_{SiO_2}^{-1}$ (see **Table 1**) whereas currently existing high-quality experimental ZTCs typically exhibit SPD_{cell} quantities of 0.32–0.40 $g_{ZTC}\, g_{SiO_2}^{-1}$.

Several strategies have been implemented to increase the SPD of ZTCs, including altering the deposition kinetics by means of pulsed chemical vapor deposition (P-CVD) [24] and reducing the diffusion path length of precursor diffusion using nano-sized zeolites [22]. The highest SPD_{cell} values achieved to date are the following: 0.53 for P-CVD and 0.68 for nano-sized zeolites (all calculated using the same method by the authors herein). However, in these cases, over-deposition occurred [22, 24] meaning that a graphitic shell was formed on the external surface of the zeolite particles, resulting in a core-shell type structure. Hence, in both cases it was difficult to assess solely the SPD of the porous ZTC network and the solid was not a homogeneous framework.

The polycyclic hydrocarbon rings formed during the synthesis of ZTCs can in principle participate in cation-π interactions [25] with the extra-framework cations present in the zeolite template. The strength of these interactions depends on the charge and size of the cations, increasing in strength as the size of the cation decreases. While multivalent cations increase the interaction strength and subsequent catalytic activity [18, 21], they also reduce the number of catalytic sites which could lead to carbon deposition heterogeneity. Therefore, in this study we aim to systematically investigate the effects of monovalent cation size on the template fidelity of **FAU**-ZTC by templating Li-, Na-, and K-exchanged variants of zeolite Y.

2. Materials & Methods

2.1 Zeolite cation exchange

Lithium-exchange was achieved using a previously reported procedure [26] by stirring 20 g of sodium-exchanged USY zeolite (HSZ-320NAA, Si:Al=11, Tosoh Corp.) in 200 mL of 1 M aqueous LiCl (99.0%, J. T. Baker) at 80 °C for 4 h. The Li-exchanged zeolite was then filtered using cellulose filter paper (8 µm, Whatman 1002090), rinsed with water, dried under suction for 10 min, and then further dried at 80 °C for 12 h. The dried zeolite was then placed in an alumina boat (10×30×107 mm) which was inserted into a quartz tube (ϕ45 mm) installed in a horizontal tube furnace (HST 12/600, Carbolite Gero) and heated to 350 °C at 1 °C per min, under flowing N_2 (99.999%). This procedure (comprising a single exchange step) was repeated five times in total. After each exchange step, 4 g of partially-

Table 1 SPD, BET surface area (SA), and pore volume of ZTCs synthesized from cation-exchanged **FAU** zeolite templates compared to benchmark ZTC models.

Material/Model	SPD_{cell} ($g_{ZTC}\ g_{SiO_2}^{-1}$)	ZTC BET SA ($m^2\ g^{-1}$)	ZTC Pore Volume ($mL\ g^{-1}$)	C (at %)	H (at %)	O (at %)
LiY5 ZTC	0.40	3360	1.57	78.4%	14.7%	6.4%
NaY ZTC	0.39	3560	1.60	78.6%	15.7%	5.3%
KY5 ZTC	0.35	3650	1.76	80.5%	15.7%	4.6%
Nishihara Model II+ [29, 30]	0.35	4290	1.61	71.2%	23.8%	5.0%
Braun Model R [19]	0.68	1600	0.62	100%	0%	0%

exchanged zeolite were collected and a 10 : 1 ratio of LiCl solution volume to zeolite mass was maintained.

Potassium-exchange was achieved using a similar procedure as that described above. Since potassium can exchange with sodium more readily than lithium [27], the concentration of potassium in each exchange solution was altered to create a diverse series of potassium-exchanged zeolites. This series was created by varying the volume ratio within a mixture of 1 M aqueous KCl (99.7%, Fisher Chemical) and 1 M aqueous NaCl (99.7%, Fisher Chemical). Mixtures containing volume ratios of 20 : 80, 40 : 60, 60 : 40, 80 : 20, and 100 : 0 were prepared in an attempt to achieve an extent of potassium exchange of 20, 40, 60, 80 and 100%, respectively.

A control sample was also prepared to reveal any chemical or structural changes that could occur during the cation-exchange procedure described above. One exchange control step was performed using a similar procedure as in lithium- and potassium-exchange, with 5 g of sodium-exchanged USY zeolite in 50 mL of 1 M aqueous NaCl (99.7%, Fisher Chemical).

The cation-exchanged zeolites are named to indicate the type of cation exchanged, the letter Y to indicate the zeolite type, and which exchange step the zeolite was collected after. For example, LiY3 and KY3 are zeolite Y samples that have undergone three steps of lithium- and potassium exchange, respectively. The sodium-exchanged sample is referred to herein simply as NaY.

2.2 Zeolite-templated carbon synthesis

All ZTCs were synthesized via a 2-step method whereby 2 g of zeolite template was degassed in a glass oven (B-585, Büchi Corp.) at 300 °C for 24 h under oil-free vacuum ($<2\times10^{-3}$ mbar). The dried zeolite template was then transferred into a 2-neck round-bottom flask in an inert atmosphere and 20 mL of furfuryl alcohol (FA, 98%, Aldrich) was added via syringe. The mixture was stirred at room temperature under passive vacuum for 12 h. The impregnated solid was then collected by vacuum filtration in air, washed three times with 10 mL aliquots of mesitylene (97%, Aldrich) and dried under suction on the filter frit for 15 min. The impregnated and rinsed zeolite was then placed in an alumina boat (10×30×107 mm) which was inserted into a quartz tube (ϕ45 mm) installed in a horizontal tube furnace (HST 12/600, Carbolite Gero). The tube was purged with dry argon flow (200 sccm) and the FA within the zeolite pores was first polymerized by heating up to 80 °C at 5 °C per min and held for 24 h. The poly-FA was then carbonized by heating up to 700 °C at 5 °C per min and held for 30 min. Carbon deposition was accomplished via propylene (200 sccm, 7 mol% 99.99% propylene in 99.999% argon) CVD at 700 °C for 5 h. After ambient pressure CVD, the gas flow was returned to dry argon at 200 sccm. A heat treatment step was performed by heating the zeolite-carbon composite up to 900 °C at 5 °C per min and held for an additional 3 h. The system was then cooled overnight, the gas flow was stopped, and the annealed zeolite-carbon composite was collected. Removal of the zeolite template was accomplished by three sequential dissolutions in 35 mL of aqueous hydrofluoric acid (HF, 48–51%, Thermo Scientific). The final ZTC product was collected by centrifugation, washed three times with 35 mL aliquots of distilled water, and dried in air at 40 °C to obtain the final ZTC material. Some samples were subject to additional iterations of acid washing to ensure complete dissolution of the zeolite template, as determined by XRD.

2.3 Inductively coupled plasma optical emission spectrometry

The extent of cation exchange in each zeolite was determined via optical emission spectrometry (OES) using a benchtop inductively coupled plasma (ICP) emission spectrometer (Thermo iCAP-6500 Duo View, Thermo Scientific). Each sample of dried zeolite powder was dissolved in a series of proprietary reagents (UniSolv, Inorganic Ventures Inc.) prior to analysis [28]. First, 10 drops of water were added to 80 mg of zeolite to hydrate the sample and prevent agglomerations in a 250 mL Nalgene bottle. Then, 10 mL of UA-1 (Inorganic Ventures) and 0.5 mL of concentrated 70% nitric acid (Certified ACS Plus, Fisher Chemical) were added to the vessel, capped, and shaken for 2 min. The solution was neutralized by adding 50 mL of UNS-1 (Inorganic Ventures) and allowed to fully react. DI water was then added to achieve a final solution weight of 150 grams. To achieve homogeneity, the final solutions were mixed by inverting the capped bottles 50 times prior to further analysis.

2.4 X-ray diffraction

Powder XRD patterns were measured using Cu Kα radiation (λ= 1.54 Å), generated at 40 kV and 40 mA, in Bragg-Brentano geometry (D8 Advance, Bruker Corp.). The powder was thinly dispersed on a "low-background" sample holder comprised of oriented crystalline silicon.

2.5 Nitrogen adsorption

Nitrogen adsorption/desorption isotherms were measured at 77 K between 10^{-4} and 100 kPa using an automated volumetric instrument (3Flex, Micromeritics Instrument Corp.). Specific surface areas were calculated by Brunauer-Emmet-Teller (BET) method between P/P_0=5×10^{-7}–0.02 and P/P_0=4×10^{-6}–0.10 for zeolite and ZTC samples, respectively. Pore-size distributions were determined by nonlocal density functional theory (NLDFT) calculations using a dedicated software package (MicroActive Share, Micromeritics Instrument Corp.) with a carbon slit-pore model.

2.6 Thermogravimetric analysis

Thermogravimetric analysis (TGA) was performed using a microbalance (Discovery TGA 5500, TA Instruments) under flowing dry air at 25 mL min^{-1} (Grade D breathing air with a moisture trap) to determine the hydrocarbon content of each zeolite-carbon composite prior to HF treatment. The temperature program was specified as follows: the sample was first held at 50 °C for 15 min under dry air to purge, and then water removal was performed by heating up to 300 °C at 10 °C per min and holding for 1 h. The weight at the end of this dehydration step was taken to be the initial mass, m_i. The carbon was oxidized by heating up to 800 °C at 5 °C per min and holding for 2 h, and finally remaining sample was cooled to 300 °C and held for 1 h to determine the final weight (m_f).

2.7 Structural packing density

The SPD of each ZTC was determined using the data obtained from TGA of the corresponding zeolite-carbon composite according to Equation 1:

$$SPD_{exp} = \frac{m_{ZTC}}{m_{zeolite}} = \frac{m_i - m_f}{m_f} = g_{ZTC}\, g_{zeolite}^{-1} \quad \cdots\cdots (1)$$

In order to accurately compare the SPD across samples where the zeolite templates differ in Si:Al ratio, charge balance cation identity, or framework type all together, the SPD_{exp} must be converted to account for the subsequent differences in zeolite mass or pore volume [23]. If the same type of zeolite framework is used within a given series of samples (*e.g.*, **FAU**), SPD_{exp} can be converted to SPD_{cell} using the molecular weight of the zeolite ($MW_{zeolite}$) and the corresponding theoretical molecular weight of the pure silicate (cation free) version of the zeolite (MW_{SiO_2}), according to Equation 2:

$$SPD_{cell} = SPD_{exp} \times \frac{MW_{zeolite}}{MW_{SiO_2}} = g_{ZTC}\, g_{SiO_2}^{-1} \quad \cdots\cdots (2)$$

Example calculations are given in the Supporting Information.

2.8 Elemental analysis

Elemental composition was determined via combustion analysis (in triplicate, Atlantic Microlab Inc.) after drying the ZTC powder at 120 °C for 12 h under rough vacuum (10^{-3} mbar).

2.9 ZTC atomistic models

Two models, the Nishihara Model II+ and Braun Model R, are referenced as benchmark examples of open-blade and closed-tube atomistic renderings of **FAU**-ZTC, respectively. A carbon and hydrogen variant of Nishihara Model II was first published in 2018 [29], which has since been improved by the addition of oxygen resulting in the model most representative of experimentally obtained ZTC, referred to herein as Nishihara Model II+ [30]. A library of schwarzite-like structures which could result from perfect deposition of carbon on the inner pore surface of various zeolite templates was later published, all of which are clearly closed-tube type structures and not experimentally realized [19]. In this work, the CP2K relaxed version of the **FAU**-templated carbon (**FAU**_1_nozeolite_relaxed) is referred to as Braun Model R.

2.10 Theoretical structural properties

Open-access software (Zeo++, v.0.3) [31] was used to calculate the N_2-accessible surface area of all atomistic models assuming a channel radius and probe radius of 1.86 Å [32], with 2000 Monte Carlo samples per atom. Likewise, probe-occupiable pore volumes were calculated using the same assumptions except with 200 Monte Carlo samples per atom. All calculations were performed using the high accuracy (-ha) parameter.

3. Results

Cation exchange across a wide range of compositions (up to 58% for Li and 94% for K) was achieved using a standard aqueous solution exchange method, as shown in **Fig 3**. Lithium-exchange is thermodynamically unfavorable owing to the stronger hydration energy of lithium as compared to sodium [27]; the maximum exchange concentration (58%) achieved in this work is comparable to the replicated study [26, 33], though greater lithium exchange has been achieved using a lithium nitrate solution [34]. The potassium-exchange isotherm reaches a plateau between the third and fourth exchanges resulting in KY3 and KY4 having similar potassium exchange amounts

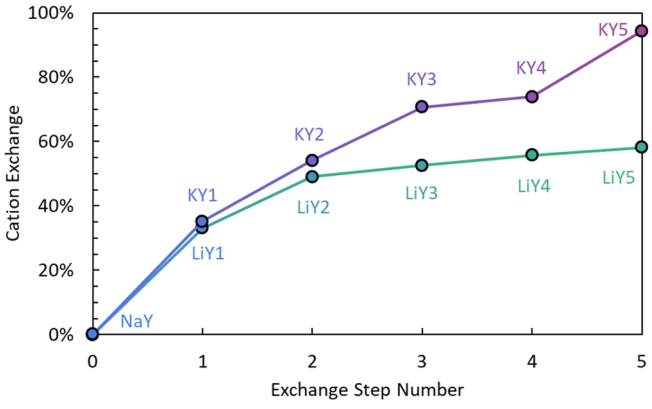

Fig. 3 Composition of cation-exchanged **FAU** zeolite templates as a function of the exchange step number, as determined using ICP-OES.

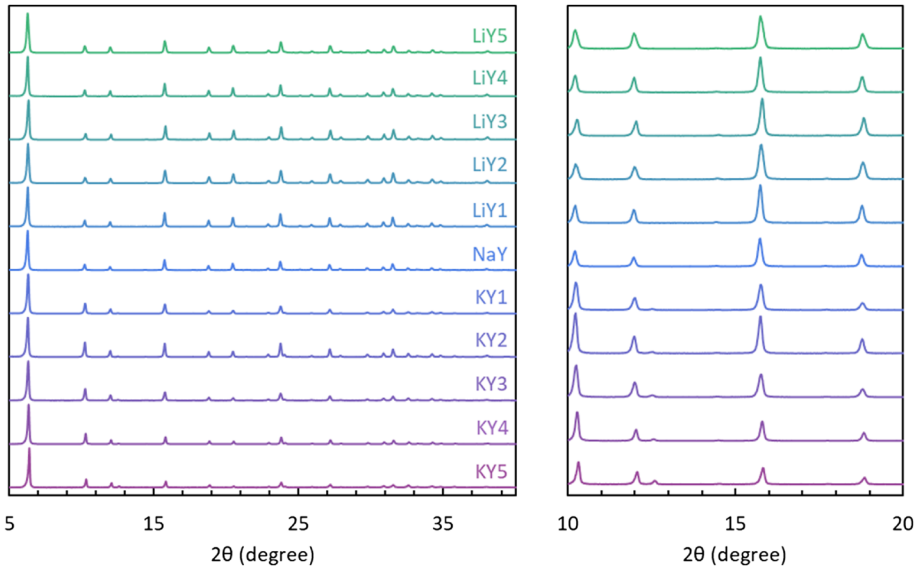

Fig. 4 XRD patterns of the cation-exchanged **FAU** zeolite templates (originally NaY).

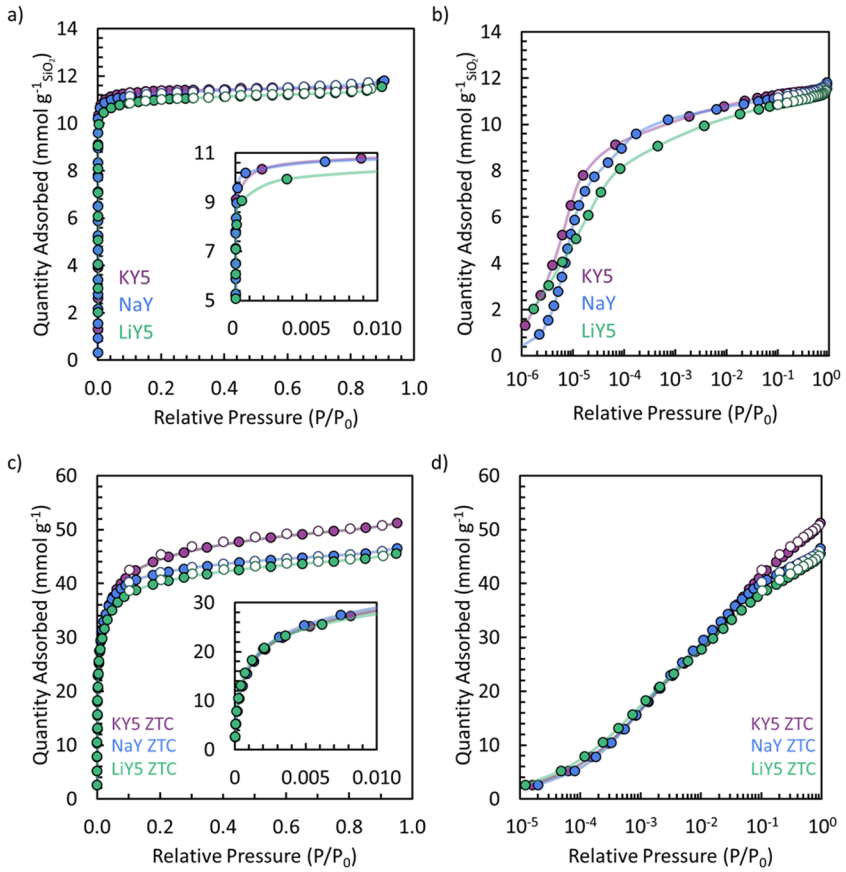

Fig. 5 Nitrogen adsorption/desorption isotherms at 77 K of (a, b) select cation-exchanged **FAU** zeolite templates, converted to mmol g^{-1}_{SiO2}, and (c, d) the corresponding ZTCs.

[35]. Unlike lithium-exchange, complete potassium-exchange is eventually possible as previously reported [17, 34, 36–38].

The periodic structural integrity of the zeolite templates was maintained during cation exchange, without the loss of any characteristic XRD reflections, as shown in **Fig. 4**. The (222) reflection centered at 2θ=12.6° intensifies upon potassium exchange at high concentrations

Table 2 BET surface area (SA) and pore volume of cation-exchanged **FAU** zeolite templates.

Zeolite	Zeolite BET SA ($m^2\ g^{-1}_{SiO_2}$)	Zeolite Pore Volume ($mL\ g^{-1}_{SiO_2}$)
LiY5	1000	0.40
NaY	1040	0.41
KY5	1050	0.40

owing to the larger scattering cross-section of K^+ compared to Na^+ and Li^+ [39]. Some structural differences between the three cation-exchanged zeolites are evident by analysis of the nitrogen adsorption isotherms at 77 K (see **Fig. 5**). The pore volume decreases slightly upon incorporation of lithium and potassium (**Table 2**). Likewise, the pore size distribution of the cation-exchanged zeolites is also affected by cation identity; the larger pores present in LiY5 (~8.0 Å in width) are revealed to decrease in prevalence as the cation size increases, as exemplified by comparison to NaY and KY5 (**Fig. 6**).

Despite the minor differences in porosity of the templates as a function of cation exchange, no major change is evident in the periodic structure of the resulting ZTCs, as shown in **Fig. 7**. All of the ZTCs exhibit a sharp (111) reflection at ~6.5° in 2θ and the presence of a minor (220) reflection at ~10.6° in 2θ indicating high pore-to-pore regularity and the same pore-to-pore spacing. Notably, no graphitic stacking is observed (expected at ~26° in 2θ) which is typically the result of carbon deposition on the outer surfaces of the zeolite particles. Interestingly, once again, the nitrogen adsorption measurements reveal some differences between the ZTCs resulting from different cation exchange. As the size of the cation increases, surface area and pore volume also increase, as seen in **Fig. 5** and **Table 1**. The opposite trend is observed for SPD_{cell}, where carbon deposition within the zeolite template (slightly) increases with decreasing cation size (**Fig. 8** and **Table 1**). Lastly, combustion analysis (see **Table 1**) of the resulting ZTC samples shows a higher concentration of carbon in the overall chemical composition of KY5 ZTC when compared to both LiY5 ZTC and NaY ZTC, and a reversed trend for oxygen. The trends in SPD_{cell} and chemical composition, while subtle in magnitude, are a credible body of results as a whole.

4. Discussion

Achieving schwarzite-like ZTCs necessitates the formation of closed-tube carbon struts within the confined pore spaces of the zeolite template. Currently existing ZTCs, such as all of the materials produced in the present work, exhibit far lower carbon packing

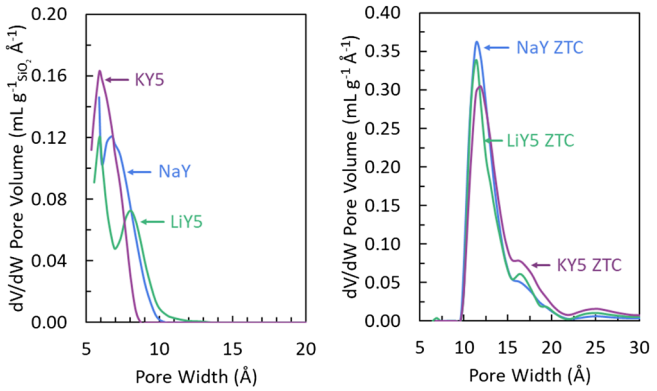

Fig. 6 NLDFT pore size distributions of the cation-exchanged **FAU** zeolite templates, converted to mL g_{SiO2}^{-1} $Å^{-1}$ (left) and corresponding ZTC samples (right).

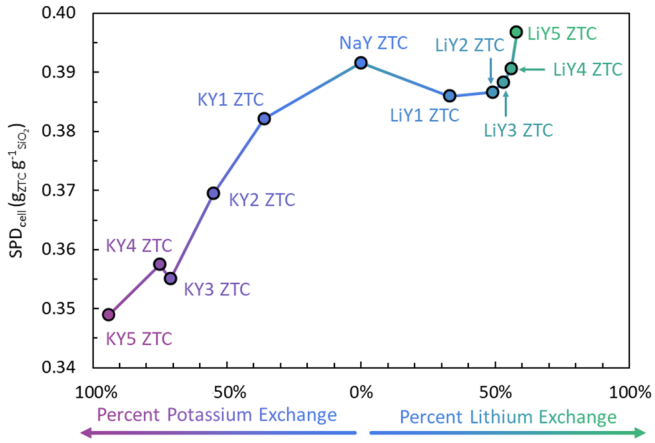

Fig. 8 SPD_{cell} plotted as a function of percent cation exchange in the zeolite template used to synthesize each respective ZTC.

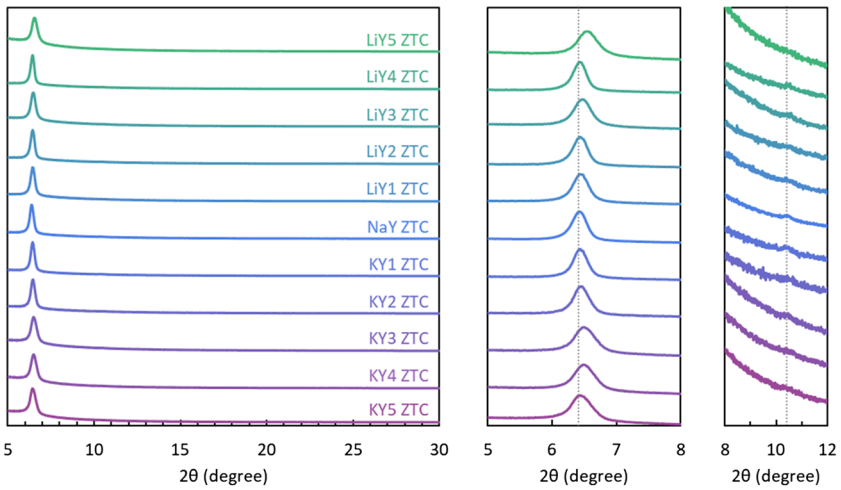

Fig. 7 XRD patterns of ZTCs synthesized from cation-exchanged **FAU** zeolite templates. No internal standard was used to correct for sample height error.

(SPD_{cell} $\leq 0.40\, g_{ZTC}\, g_{SiO_2}^{-1}$) and far higher surface area (BET SA $>3000\ m^2\ g^{-1}$) than would be predicted for such materials, as shown in **Table 1**. As carbon packing within the zeolite gradually increases toward this goal, surface area and pore volume, as measured by a nitrogen molecular probe, would eventually be expected to decrease. Eventually, the formation of fully enclosed closed-tube struts would be expected to result in a surface area of less than half that of the open-blade variant as the pore space on the inner side of the struts becomes inaccessible to N_2. Such structures also comprise relatively more carbon than open-blade networks, imparting a higher SPD_{cell}. Lastly, however, it must be noted that an increase in SPD_{cell} can also simply occur via undesirable graphitic carbon deposition (graphitic stacking) on the outer particle surfaces, a form of contamination of the ordered porous ZTC structure. In summary, the figure of merit known as SPD_{cell} is a worthwhile indicator of increasingly schwarzite-like ZTCs, but must be interpreted with care owing to its complex relationship with the other key properties of ZTCs and schwarzites.

According to the above discussion, the analysis of ZTC structure requires the use of combination of at least three characterization techniques together: diffraction, TGA, and elemental analysis. For example, a lower surface area could either be indicative of poor template fidelity leading to collapse of the atomically thin carbon walls upon zeolite removal, or it could signal the disappearance of edge sites and an improvement in carbon deposition within the zeolite. In severe instances, the former case can be confirmed using powder XRD to detect graphitic stacking, while the latter can be verified using combustion analysis. As ZTCs consist of entirely sp^2-hybridized carbon [40], hydrogen and oxygen must terminate edge sites of a graphene ribbon-like blade. The decrease in hydrogen content (**Table 1**) in accompaniment with lower BET surface area and pore volume signifies the disappearance of edge sites in LiY5 ZTC. Oxygen functional groups could also terminate edge sites; however, a majority of the oxygen contamination is proposed to originate from σ radicals, which are originally stabilized by the zeolite pore walls, and ultimately quenched by oxygen during the zeolite removal process [41]. Therefore, the increase in oxygen content could imply a ZTC structure which is templated closer to the zeolite pore wall. In comparison, KY5 ZTC exhibits both a higher BET surface area and pore volume with lower SPD_{cell} and oxygen content, indicating an open-blade structure templated mainly in the pore volume of the zeolite template, as the reduced catalytic activity of the zeolite slows carbon deposition and the decreased zeolite pore size spatially restricts the introduction of carbon within the zeolite pores.

The observed difference in oxygen content between ZTCs insinuates future complications in the synthesis of high template fidelity ZTCs. If templating close to the zeolite walls results in the formation of σ radicals, oxygen may be inherently grafted to the structure of even high-fidelity schwarzite-like ZTCs. Therefore, a rigourous quenching of the σ radicals (*e.g.*, with hydrogen gas [41] or post-synthetic heat-treatments/modifications) may be necessary to achieve a pure carbon structure. Such studies remain outside the scope of the present work but are warranted in future efforts to decouple the oxygen content from the edge content in post-HF dissolved ZTCs. In addition, it is notable that while some structural differences are observed between LiY5 ZTC and NaY ZTC (**Table 1**), the maximum effect of lithium-exchange within zeolite Y has not yet been fully captured. The CVD conditions, which were not varied in this work, would need to be optimized to determine if even higher SPD_{cell} could be achieved without the presence of graphitic stacking on the outside of the template particles.

The hypothesis of this work was that higher SPD_{cell} could be achieved without graphitic stacking by exchanging sodium with lithium within the zeolite template, exploiting stronger cation-π interactions between the cation and the π-network of the eventual ZTC structure. While SPD_{cell} did not appreciably increase as a function of lithium-exchange, the opposite effect did occur for potassium-exchange, which could be a direct result of diminished cation-π interactions in KY templates. Likewise, the highest absolute carbon packing density achieved in this work was that for LiY5 ZTC (SPD_{cell}=0.40 $g_{ZTC}\, g_{SiO_2}^{-1}$, **Fig. 8**), the most lithium-exchanged sample. The oxygen content, as noted above, could be a further indication of slightly closer templating of the LiY5 zeolite. These facts together lend credibility to the hypothesis that it is possible to leverage the stronger cation-π interactions in Li-exchanged templates toward more schwarzite-like ZTCs, and that further work in this direction is warranted.

5. Conclusions

Lithium- and potassium-exchange across a wide range of compositions were performed within zeolite Y using a standard procedure; 58 and 100% exchange was accomplished in five exchange steps, respectively. High template fidelity ZTCs were then prepared from all templates under identical impregnation and CVD conditions without any apparent graphitic growth on the external surfaces of the zeolite particles. Minor but important trends in the properties of the resulting materials are insightful for future efforts to prepare less open-blade-like and more closed-tube-like ZTC materials. Increasing the amount of potassium in the template led to more open-blade like structures with lower SPD_{cell} and higher BET surface area and total pore volume. On the other hand, templating LiY revealed early signs of a transition to more closed-tube-like structure, with lower BET surface area and hydrogen content. Future efforts to synthesize schwarzite-like ZTCs will require optimization of the synthesis conditions within LiY templates and may also require post-synthetic treatments to scavenge σ radicals in order to obtain a higher carbon content structure.

References

[1] H.W. Kroto, J.R. Heath, S.C. O'Brien, R.F. Curl, R.E. Smalley, C_{60}: Buckminsterfullerene, Nature 318 (1985) 162–163.

[2] A. Hirsch, The era of carbon allotropes, Nat. Mater. 9 (2010) 868–871.

[3] S. Iijima, T. Ichihashi, Single-shell carbon nanotubes of 1-nm diameter, Nature 363 (1993) 603–605.

[4] K.S. Novoselov, A.K. Geim, S.V. Morozov, D. Jiang, Y. Zhang, S.V. Dubonos, I.V. Grigorieva, A.A. Firsov, Electric field effect in atomically thin carbon films, Science 306 (2004) 666–669.

[5] T. Lenosky, X. Gonze, M. Teter, V. Elser, Energetics of negatively curved graphitic carbon, Nature 355 (1992) 333–335.

[6] A.L. Mackay, H. Terrones, Diamond from graphite, Nature 352 (1991) 762.

[7] M. O'Keeffe, G.B. Adams, O.F. Sankey, Predicted new low energy forms of carbon, Phys. Rev. Lett. 68 (1992) 2325–2328.

[8] S.J. Townsend, T.J. Lenosky, D.A. Muller, C.S. Nichols, V. Elser, Structural Models of Negatively Curved Graphitic Carbon, MRS Online Proceedings Library (OPL) 270 (1992) 229–234.

[9] D. Vanderbilt, J. Tersoff, Negative-curvature fullerene analog of C_{60}, Phys. Rev. Lett. 68 (1992) 511–513.

[10] H.A. Schwarz, Gesammelte Mathematische Abhandlungen, Vol. 1, Springer Berlin, Heidelberg, 1890.

[11] A.H. Schoen, Infinite periodic minimal surfaces without self-intersections, Technical Report, NASA TN D-5541 (1970) C-98.

[12] C. Baerlocher, L.B. McCusker, Database of Zeolite Structures. http://www.iza-structure.org/databases/ (accessed July 2022).

[13] C. Baerlocher, L.B. McCusker, D.H. Olson, Atlas of Zeolite Framework Types, Elsevier, 2007.

[14] T. Kyotani, T. Nagai, A. Tomita, Preparation of new carbon from zeolite as template, Proceedings of Carbon 92 (1992) 437–478.

[15] T. Kyotani, T. Nagai, S. Inoue, A. Tomita, Formation of new type of porous carbon by carbonization in zeolite nanochannels, Chem. Mater. 9 (1997) 609–615.

[16] M. Shamzhy, M. Opanasenko, P. Concepción, A. Martínez, New trends in tailoring active sites in zeolite-based catalysts, Chem. Soc. Rev. 48 (2019) 1095–1149.

[17] T. Frising, P. Leflaive, Extraframework cation distributions in X and Y faujasite zeolites: A review, Microporous Mesoporous Mater. 114 (2008) 27–63.

[18] K. Kim, T. Lee, Y. Kwon, Y. Seo, J. Song, J.K. Park, H. Lee, J.Y. Park, H. Ihee, S.J. Cho, R. Ryoo, Lanthanum-catalysed synthesis of microporous 3D graphene-like carbons in a zeolite template, Nature 535 (2016) 131–135.

[19] E. Braun, Y. Lee, S.M. Moosavi, S. Barthel, R. Mercado, I.A. Baburin, D.M. Proserpio, B. Smit, Generating carbon schwarzites via zeolite-templating, Proc. Natl. Acad. Sci. U.S.A. 115 (2018) E8116–E8124.

[20] H. Lee, K. Kim, S.-H. Kang, Y. Kwon, J.H. Kim, Y.-K. Kwon, R. Ryoo, J.Y. Park, Extremely high electrical conductance of microporous 3D graphene-like zeolite-templated carbon framework, Sci. Rep. 7 (2017) 11460.

[21] G. Yang, L. Li, H. Liu, Y. Cheng, Y. Chen, X. Li, Metal ion (Ca^{2+}, Mg^{2+}, Zn^{2+}) catalyzed synthesis of high-quality zeolite templated carbon, Microporous Mesoporous Mater. 336 (2022) 111860.

[22] P. Boonyoung, T. Kasukabe, Y. Hoshikawa, Á. Berenguer-Murcia, D. Cazorla-Amorós, B. Boekfa, H. Nishihara, T. Kyotani, K. Nueangnoraj, A. Simple, "Nano-Templating" Method Using Zeolite Y Toward the Formation of Carbon Schwarzites, Front. Mater. 6 (2019) 104.

[23] E.E. Taylor, K. Garman, N.P. Stadie, Atomistic Structures of Zeolite-Templated Carbon, Chem. Mater. 32 (2020) 2742–2752.

[24] K. Nueangnoraj, H. Nishihara, K. Imai, H. Itoi, T. Ishii, M. Kiguchi, Y. Sato, M. Terauchi, T. Kyotani, Formation of crosslinked-fullerene-like framework as negative replica of zeolite Y, Carbon 62 (2013) 455–464.

[25] J.C. Ma, D.A. Dougherty, The cation−π interaction, Chem. Rev. 97 (1997) 1303–1324.

[26] G. Maurin, Y. Belmabkhout, G. Pirngruber, L. Gaberova, P. Llewellyn, CO_2 adsorption in LiY and NaY at high temperature: molecular simulations compared to experiments, Adsorption 13 (2007) 453–460.

[27] M. Jeffroy, A. Boutin, A.H. Fuchs, Understanding the Equilibrium Ion Exchange Properties in Faujasite Zeolite from Monte Carlo Simulations, J. Phys. Chem. B 115 (2011) 15059–15066.

[28] P. Gaines, Elemental Analysis of Zeolites. https://www.inorganicventures.com/guides-and-papers/elemental-analysis-of-zeolites (accessed 4 August 2022).

[29] H. Nishihara, H. Fujimoto, H. Itoi, K. Nomura, H. Tanaka, M.T. Miyahara, P.A. Bonnaud, R. Miura, A. Suzuki, N. Miyamoto, N. Hatakeyama, A. Miyamoto, K. Ikeda, T. Otomo, T. Kyotani, Graphene-based ordered framework with a diverse range of carbon polygons formed in zeolite nanochannels, Carbon 129 (2018) 854–862.

[30] K. Nomura, H. Nishihara, M. Yamamoto, A. Gabe, M. Ito, M. Uchimura, Y. Nishina, H. Tanaka, M.T. Miyahara, T. Kyotani, Force-driven reversible liquid–gas phase transition mediated by elastic nanosponges, Nat. Commun. 10 (2019) 1–10.

[31] T.F. Willems, C.H. Rycroft, M. Kazi, J.C. Meza, M. Haranczyk, Algorithms and tools for high-throughput geometry-based analysis of crystalline porous materials, Microporous Mesoporous Mater. 149 (2012) 134–141.

[32] D. Ongari, P.G. Boyd, S. Barthel, M. Witman, M. Haranczyk, B. Smit, Accurate Characterization of the Pore Volume in Microporous Crystalline Materials, Langmuir 33 (2017) 14529–14538.

[33] T. Yashima, H. Suzuki, N. Hara, Decomposition of 2-propanol over alkali cation exchanged zeolites, J. Catal. 33 (1974) 486–492.

[34] J.W. Ward, A spectroscopic study of the surface of zeolite Y: the adsorption of pyridine, J. Colloid Interface Sci. 28 (1968) 269–278.

[35] Y. Khabzina, C. Laroche, C. Pagis, D. Farrusseng, Monovalent and bivalent cations exchange isotherms for faujasites X and Y, Phys. Chem. Chem. Phys. 19 (2017) 17242–17249.

[36] W.J. Mortier, H.J. Bosmans, Location of univalent cations in synthetic zeolites of the Y and X type with varying silicon to aluminum ratio. I. Hydrated potassium exchanged forms, J. Phys. Chem. 75 (1971) 3327–3334.

[37] M.L. Costenoble, W.J. Mortier, J.B. Uytterhoeven, Location of cations in synthetic zeolites X and Y. Part 4.—Exchange limiting factors for Ca2+ in zeolite Y, J. Chem. Soc., Faraday Trans. I 72 (1976) 1877–1883.

[38] J.W. Ward, Spectroscopic study of the surface of zeolite Y. II. Infrared spectra of structural hydroxyl groups and adsorbed water on alkali, alkaline earth, and rare earth ion-exchanged zeolites, J. Phys. Chem. 72 (1968) 4211–4223.

[39] F. Biggs, R. Lighthill, Analytical approximations for X-ray cross sections III, United States, 1988-08-01, 1988.

[40] H. Nishihara, Q.-H. Yang, P.-X. Hou, M. Unno, S. Yamauchi, R. Saito, J.I. Paredes, A. Martínez-Alonso, J.M.D. Tascón, Y. Sato, M. Terauchi, T. Kyotani, A possible buckybowl-like structure of zeolite templated carbon, Carbon 47 (2009) 1220–1230.

[41] H. Nishihara, K. Imai, H. Itoi, K. Nomura, K. Takai, T. Kyotani, Formation mechanism of zeolite-templated carbons, Tanso 2017 (2017) 169–174.